Analytica Chimica Acta 1191 (2022) 339346

Contents lists available at ScienceDirect

Analytica Chimica Acta

journal homepage: www.elsevier.com/locate/aca

Sensitive electrochemiluminescence biosensing of polynucleotide kinase using the versatility of two-dimensional $Ti_3C_2T_X$ MXene nanomaterials

Lun Wang [a, 1], Huixin Zhang [a, 1], Tingting Zhuang [a], Jingxu Liu [a], Neso Sojic [b, c], Zonghua Wang [a, *]

[a] College of Chemistry and Chemical Engineering, College of Materials Science and Engineering, Shandong Sino-Japanese Center for Collaborative Research of Carbon Nanomaterials, Instrumental Analysis Center of Qingdao University, Institute of Biomedical Engineering, Qingdao University, Qingdao, Shandong, 266071, China

[b] University of Bordeaux, Bordeaux INP, ISM, UMR CNRS 5255, Pessac, 33607, France

[c] Department of Chemistry, South Ural State University, Chelyabinsk, 454080, Russian Federation

HIGHLIGHTS

- In situ formation of Ti_3C_2Tx-AuNPs provide electrocatalytic rooting in Ti and Au.
- $Ru(bpy)_3^{2+}$ was immobilized on the Ti_3C_2Tx-AuNPs to obtain probe of Ru − Ti_3C_2Tx -AuNPs.
- DNA phosphorylated with PNK can be recognized by the chelation between Ti and PO_4^{3-}.
- A sensitive and selective ECL biosensor was constructed for the detection of PNK.

GRAPHICAL ABSTRACT

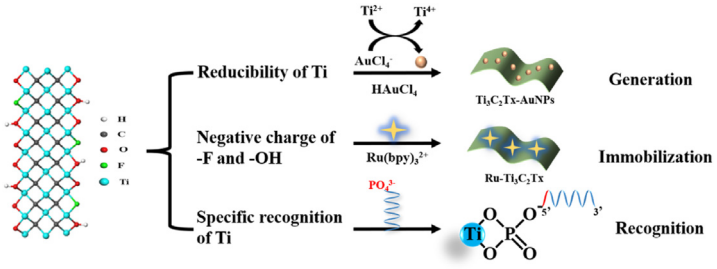

ARTICLE INFO

Article history:
Received 11 October 2021
Received in revised form
29 November 2021
Accepted 30 November 2021
Available online 9 December 2021

Keywords:
Electrochemiluminescence
$Ti_2C_3T_X$ MXene material
Biosensor
Polynucleotide kinase

ABSTRACT

Electrochemiluminescence (ECL) is a powerful readout method for the development of (bio)sensors, whose performances depend on the electrode materials and the architecture of its surface. Herein, we demonstrate that the precise control of the sensing interface using the versatility of two-dimensional (2D) transition metal carbides ($Ti_3C_2T_X$ MXene) leads to the enhancement of the ECL signal. This electrode material, which exhibits remarkable structural and electrochemical properties was decorated by the in situ formation of gold nanoparticles (AuNPs) owing to the Ti reducibility. Then, a large amount of the luminophore, $Ru(bpy)_3^{2+}$, was immobilized on $Ti_3C_2T_X$ MXene thanks to its unique negative charge and large specific surface area to obtain Ru−$Ti_3C_2T_X$-AuNPs. The presented approach exploits the high catalytic activity and excellent conductivity of this 2D nanomaterial as illustrated by the enhanced ECL emission performance of the Ru−$Ti_3C_2T_X$-AuNPs nanoprobes. Finally, DNA phosphorylated with polynucleotide kinase (PNK) was recognized efficiently by the chelation between Ti and phosphate group. A highly sensitive and selective ECL biosensor was developed for the detection of PNK and the screening of its inhibitors. A lower detection limit of 0.0002 U mL^{-1} and wide linear relationship ranged from 0.002 to 10 U mL^{-1} were obtained. Furthermore, the practicality of our method was tested in MCF-7 cell lysate, which opens enticing perspectives for future applications of $Ti_3C_2T_X$ materials in the ECL bioanalysis field.

© 2021 Elsevier B.V. All rights reserved.

* Corresponding author.
E-mail address: wangzonghua@qdu.edu.cn (Z. Wang).

[1] Lun Wang and Huixin Zhang contribute equally to this work.

https://doi.org/10.1016/j.aca.2021.339346
0003-2670/© 2021 Elsevier B.V. All rights reserved.

1. Introduction

Electrochemiluminescence (ECL) is a sensitive analytical method, which combines the advantages of electrochemistry and chemiluminescence [1–5]. It provides high sensitivity, low cost, wide dynamic range, easy controllability and simple instrumentation with portable devices [6–12]. Developing sensitive and selective interfaces of ECL biosensors and improving ECL intensity are central issues in this field [13–16]. Much efforts have been expended with in-depth works to improve the analytical performances of ECL [17–22]. On the one hand, the development of new luminophores and coreactant species further increases the efficiency of ECL [23–31]. On the other hand, based on the novel recognition method and the construction strategy of biosensor interface, the correlation between the target molecule and the response signal is established to further enhanced the performance of ECL biosensor [32–34]. For instance, a novel ECL sensor was developed for the detection of kinase activity based on multifunctional nanoprobes and the recognition of Zr^{4+} and phosphate [35]. These examples illustrate the importance of developing well-controlled interfaces and nanomaterials for effective ECL biosensing.

The design and fabrication of efficient and simple ECL analytical systems is a challenging but highly rewarding task. A large variety of nanomaterials from carbon based to quantum dots, metallic nanoparticles or carbon oxides has been reported for ECL detection [36–40]; each of them providing distinct advantages. Among them, the 2D transition metal carbide $Ti_3C_2T_X$ ($Ti_3C_2T_X$, Tx includes O, OH, and/or F) is a relatively new class of materials [41,42]. It presents unique layered structure and surface chemical properties, and its characteristics show promising potential for electroanalytical applications [43]. For example, $Ti_3C_2T_X$ was used to form composite film with Nafion for fabrication of a solid-state ECL sensor [44]. Kerr and coworkers demonstrated the bright cathodic ECL emission using $Ru(bpy)_3^{2+}$/peroxydisulfate at pure $Ti_3C_2T_X$ electrodes [45]. Sun et al. reported that $Ti_3C_2T_X$ promotes the transfer of electrons on the electrode interface and alleviates the passivation of g-C_3N_4, generating high and stable ECL signal [46]. A sensitive ECL biosensor for exosomes and their surface proteins was developed by in situ formation of gold nanoparticles (AuNPs)-decorated Ti_3C_2 MXene as nanoprobe, which showed excellent conductivity and catalytic effects, enhancing the ECL intensity of luminol [47]. The unique features of $Ti_3C_2T_X$ make them promising in fabrication of ECL with remarkable performances. $Ti_3C_2T_X$ material not only has the common advantages, such as large specific surface area and conductivity, but also shows specific properties due to the surface structure [48–50]. Indeed, $Ti_3C_2T_X$ shows excellent reducibility owing to the Ti atoms that are easily oxidized to +4. Moreover, the rich Ti vacancy defects resulting that $Ti_3C_2T_X$ nanosheets has excellent catalytic activity and the Ti atoms are easy to combine with other groups [51]. Meanwhile, the −F and −OH terminated groups make Ti_3C_2Tx negatively charged and offers good hydrophilicity [52–54]. $Ti_3C_2T_X$ MXenes have attracted increasing attention for electrochemical and ECL sensing [55]. Applying $Ti_3C_2T_X$ versatility to ECL biosensing is a very interesting approach.

Herein, a pleiotropic ECL biosensor for the highly sensitive and selective detection of PNK was designed based on the functionalization of the $Ti_3C_2T_X$ platform (Scheme 1). PNK is an enzyme isolated from *E. coli* infected by T even-numbered bacteriophages and plays a vital role in phosphorylation-related DNA repair. The abnormal expression of PNK is related to many diseases, such as Rosemond-Thomson syndrome, cardiovascular disease, central nervous system disorders and so on [56]. Therefore, it is of great significance to monitor PNK activity for clinical diagnoses and fundamental biochemical research. The $Ti_3C_2T_X$ nanosheets as the effective substrates achieve in situ generation of AuNPs anchored on $Ti_3C_2T_X$ to form $Ti_3C_2T_X$-AuNPs via the reducibility of Ti. According to the $Ti_3C_2T_X$ negatively charged, the Ru−$Ti_3C_2T_X$-AuNPs was obtained via the electrostatic interactions between $Ti_3C_2T_X$ and $Ru(bpy)_3^{2+}$. Noticeably, the obtained Ru−$Ti_3C_2T_X$-AuNPs nanoprobes exhibit a stable and bright ECL emission. The Ru−$Ti_3C_2T_X$-AuNPs nanoprobes was finally functionalized by the phosphorylated DNA efficiently due to the chelation interactions between the Ti sites enriched and the phosphate groups.

In this strategy, AuNPs modified on electrode interface can provide more binding sites for linking single stranded DNA with sulfhydryl group. Based on the specific catalysis of PNK, an enzyme isolated from *E. coli* infected and playing a vital role in phosphorylation-related DNA repair; the 5′-OH terminal of DNA is phosphorylated by ATP adenosine. This fabricated ECL biosensor shows significant improvements in detecting PNK with high sensitivity and selectivity as shown for the activity determination of PNK in cell lysate. This will provide a prospect for the design of signal amplification and specific recognition strategies based on $Ti_3C_2T_X$ material.

2. Experimental section

2.1. Materials and apparatus

The subsection of materials and apparatus are supplied in supplementary information.

2.2. Preparation of AuNPs, $Ti_3C_2T_X$ and Ru−Ti_3C_2Tx-AuNPs

The production of AuNPs, $Ti_3C_2T_X$ [46] and Ru−$Ti_3C_2T_X$-AuNPs is described in detail in the supplementary material.

2.3. Fabrication of the ECL biosensor

Electrochemical measurements were performed in a standard glass cylindrical cell with a conventional three-electrode system, including a glassy carbon electrode (GCE), platinum sheets, silver−silver chloride (Ag/AgCl) in saturated KCl as the working electrode, counter electrode, reference electrode, respectively. $[Fe(CN)_6]^{4-/3-}$ in 0.1 M KCl solution (pH 7.0) as electrolyte was used to record the cyclic voltammograms and electrochemical impedance spectra (Fig. S4). A 0.1 M phosphate buffer solution (PBS) at pH 7.4 containing 10 mM tripropylamine (TPA) as a coreactant was used for all the ECL experiments. A glassy carbon electrode (GCE, diameter of 3 mm) was carefully polished with Al_2O_3 powder, and then ultrasonically cleaned in ethanol and DI water. Finally, it was dried with N_2. Then, 6 μL AuNPs solution was added to the surface of the GCE and dried at room temperature (AuNPs/GCE). The AuNPs/GCE was immersed in DNA (1 μM) for 24 h and incubated in MCH solution for 2 h (DNA/AuNPs/GCE). After that, it was incubated in different concentrations of PNK and 1 mM ATP (v/v = 1:1) for 1 h at 37 °C. Finally, the modified electrode (P-DNA/AuNPs/GCE) was incubated in 40 μL Ru−$Ti_3C_2T_X$-AuNPs nanoprobes for 2.5 h to obtain the ECL biosensor. Each of the above steps required cleaning the electrodes with Tris-HCl and blowing dry with N_2 to remove non-specific adsorption.

3. Results and discussion

3.1. Characterization of Ru−$Ti_3C_2T_X$-AuNPs

$Ti_3C_2T_X$ nanosheets are the starting material that was

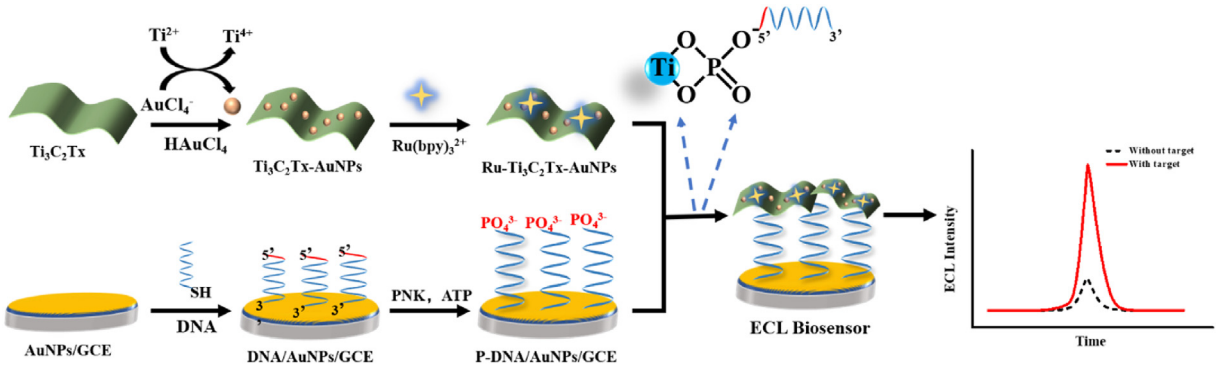

Scheme 1. Schematic representation of the fabrication and function of the ECL biosensor for PNK activity detection based on the $Ti_3C_2T_X$ nanosheets.

functionalized step by step as represented on Scheme 1. AuNPs were generated in situ by the reduction of $HAuCl_4$ thanks to the surface reducibility of Ti. It is interesting to notice that this step could be controlled by tuning the surface reducibility of $Ti_3C_2T_X$ MXene by N doping [56]. The AuNPs were anchored on the nanosheets resulting in the generation of $Ti_3C_2T_X$-AuNPs. Both $Ti_3C_2T_X$ and $Ti_3C_2T_X$-AuNPs materials were synthesized and characterized thoroughly. The XRD patterns were recorded after each fabrication step as shown in Fig. S1A. Compared with the XRD pattern of Ti_3AlC_2, the main peak (104) almost disappeared and the (002) peak shifted to the left owing to the enlarged interlayer of the $Ti_3C_2T_X$, which shows that $Ti_3C_2T_X$ had been successfully synthesized. Fig. S1B shows the specific diffraction peaks of Au, such as (111), (200), (220) and (311); they correspond to the facets diffraction peaks of face-centered cubic Au. The results show that $Ti_3C_2T_X$-AuNPs was effectively obtained. In addition, the successful preparation of $Ti_3C_2T_X$-AuNPs was confirmed by TEM. Fig. S1B demonstrates that the $Ti_3C_2T_X$ nanosheets were decorated with the AuNPs.

The next step was the modification of the synthesized nanosheets with the luminophore. It was achieved by the electrostatic interactions between $Ru(bpy)_3^{2+}$ and the negatively-charged $Ti_3C_2T_X$. The synthesis of Ru—$Ti_3C_2T_X$-AuNPs was characterized by the measurements of the zeta potential, energy dispersive spectrometer (EDS), UV—Vis and XPS. In Fig. 1A, the Ti_3C_2Tx-AuNPs synthesized in situ exhibit a less negative zeta potential value in comparison to $Ti_3C_2T_X$, with a negative potential difference of about 30 mV. The Ru—$Ti_3C_2T_X$-AuNPs shows the less negative zeta potential (d) due to the immobilization of $Ru(bpy)_3^{2+}$ with positive charges (c). The EDS spectra are displayed on Fig. 1B where the Ti, Au and Ru elements are clearly imaged on the Ru—$Ti_3C_2T_X$-AuNPs.

Fig. S2A compares the UV—Vis spectra of $Ti_3C_2T_X$ and Ru—$Ti_3C_2T_X$-AuNPs. This latter displays three characteristic peaks at 550 nm, 450 nm and 280 nm (curve b), which are the typical peaks of AuNPs, $Ru(bpy)_3^{2+}$ and $Ti_3C_2T_X$, respectively. Similarly, XPS analysis (Fig. S2B) was performed on the Ru—$Ti_3C_2T_X$-AuNPs nanosheets. Compared with Ti_3C_2Tx (Fig. S2B a), Au and Ru appeared in the spectrum of Ru—$Ti_3C_2T_X$-AuNPs nanoprobes (Fig. S2B b). To be specific, the XPS spectrum of Ti (IV) can be clearly seen in Fig. 2A at 458.6 eV and 464.3 eV. The characteristic of Au(0) reduction structure leads to the Ru—$Ti_3C_2T_X$-AuNPs composite peaks at 83.8 eV and 87.5 eV (Fig. 2B). Meanwhile, the peaks at 280.8 eV and 284.8 eV in Figs. 2C and 458.6 eV and 464.3 eV in Fig. 2D are the characteristic peaks of the Ru element. These results further indicate that Ru—$Ti_3C_2T_X$-AuNPs were successfully prepared. Fig. S3A shows the ECL spectra of $Ru(bpy)_3^{2+}$ (a) and Ru—$Ti_3C_2T_X$-AuNPs (b) in presence of tripropylamine (TPA) coreactant. The wavelength of the ECL emission peaks at about 610 nm, which is typical for the metal-to-ligand charge transfer (MLCT) emission of the $Ru(bpy)_3^{2+}$ luminophore. This means that the structure of $Ru(bpy)_3^{2+}$ remains almost unchanged after bonding with $Ti_3C_2T_X$-AuNPs. Furthermore, the stability of Ru—$Ti_3C_2T_X$-AuNPs nanoprobes were checked by recording the ECL signal during successive potential scans between 0 V and 1.25 V. The ECL process follows the well-known oxidative-reduction pathway with the model TPA coreactant. It involves the oxidation of both luminophore and coreactant (i.e. $Ru(bpy)_3^{2+}$ and TPA, respectively). The deprotonation of the electrogenerated TPA radical produces a strong reductive species that reacts very exergonically with the luminophore to generate its excited state [3—5]. A reproducible ECL strength was obtained under continuous scanning, showing good stability of Ru—$Ti_3C_2T_X$-AuNPs (Fig. S3B) thanks to the strong electrostatic interactions (*vide supra*).

3.2. Electrochemical characterizations of the assembly processes of the biosensor

The experimental detail was described in the supplementary material (Fig. S4).

3.3. ECL performance of Ru—$Ti_3C_2T_X$-AuNPs nanoprobes

In order to investigate the analytical properties of the Ru—$Ti_3C_2T_X$-AuNPs nanoprobes, a series of control experiments was carried out. A control experiment was performed without the in situ synthesis step of AuNPs to verify their catalytic ability. The ECL intensity without AuNPs (a) is lower than in presence (b) (Fig. 3A). The result confirms that the higher ECL signal of Ru—$Ti_3C_2T_X$-AuNPs/P-DNA/AuNPs/GCE is related to the in situ generation of AuNPs and decoration to form $Ti_3C_2T_X$-AuNPs via the Ti reducibility. Fig. 3B displayed the ECL performances of modified electrodes step by step. The designed biosensor shows the highest ECL intensity (curve e) compared with the others (curve a, b, c, d). These results are attributed to the electrostatic immobilization of a large amount of $Ru(bpy)_3^{2+}$ luminophores and to the large specific surface area of $Ti_3C_2T_X$. In addition, the 5′-hydroxyl terminal of DNA phosphorylated by ATP adenosine with the specific catalysis of PNK could be trapped on the modified electrode surface by specifically recognizing phosphate to produce high ECL intensity.

3.4. Activity determination of PNK

The detection conditions were optimized in Fig. S5. The ECL signal enhanced gradually with an increasing concentration of PNK as shown in Fig. 4A. It exhibited a linear relationship between the ECL strength and the concentration of PNK within the range

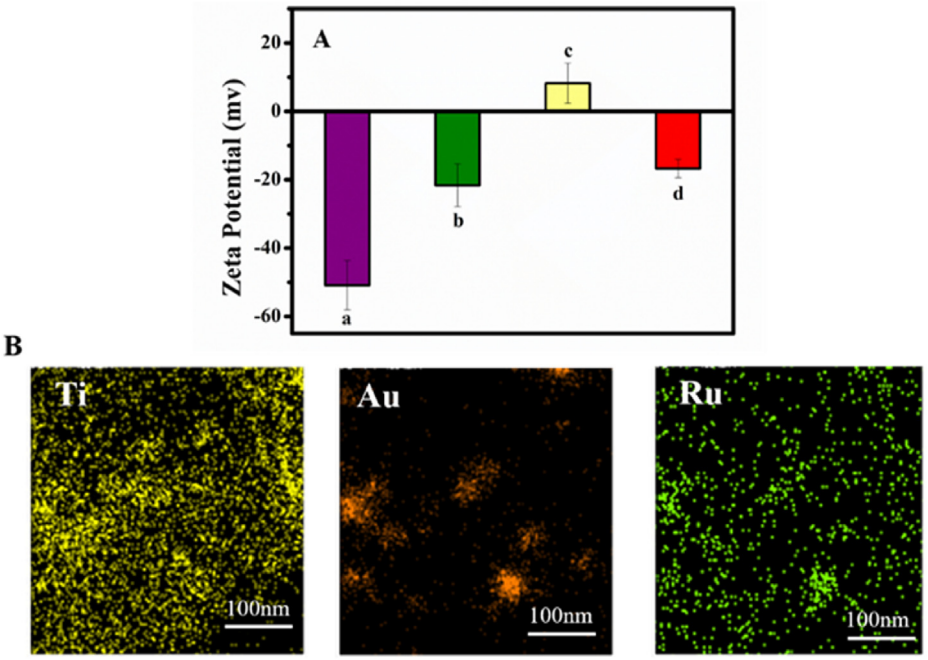

Fig. 1. (A) The zeta potential values of $Ti_3C_2T_X$ (a), $Ti_3C_2T_X$-AuNPs (b), $Ru(bpy)_3^{2+}$ (c) and Ru–$Ti_3C_2T_X$-AuNPs (d). (B) The elemental mapping of Ti element, Au element and Ru element in the Ru–$Ti_3C_2T_X$-AuNPs.

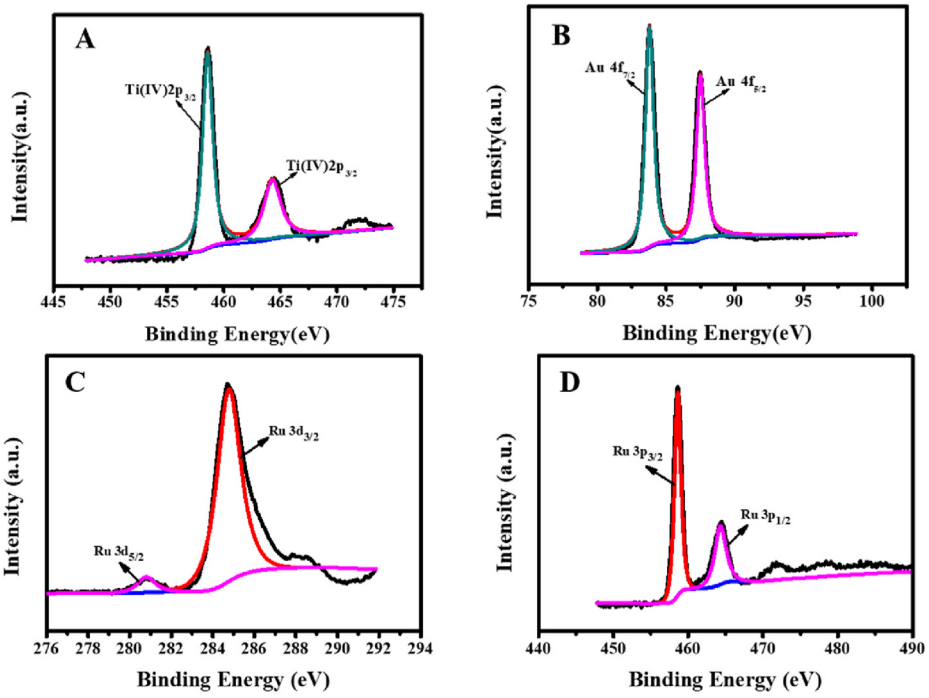

Fig. 2. The XPS spectrum of Ti (A), Au (B) and Ru (C) elements and (D) in the Ru–$Ti_3C_2T_X$-AuNPs.

0.002–10 U mL^{-1}. The equation of linear regression is $I_{ECL} = 382.86 C_{PNK}+1517.04$ (Fig. 4B). The detection limit was 0.0002 U mL^{-1} with a correlation coefficient of $R^2 = 0.987$. The analytical performance of the proposed ECL biosensor with multi-function and integration is superior to most of the work reported recently as illustrated in Table S1.

3.5. Selectivity and stability of ECL biosensor

To evaluate the selectivity of ECL biosensor, bovine serum albumin (BSA), glucose oxidase (GOD) and lysozyme at high concentrations was employed (Fig. 5A). The designed sensor shows optimal ECL response for PNK compared with the other species even at higher concentrations. These results reveal that the

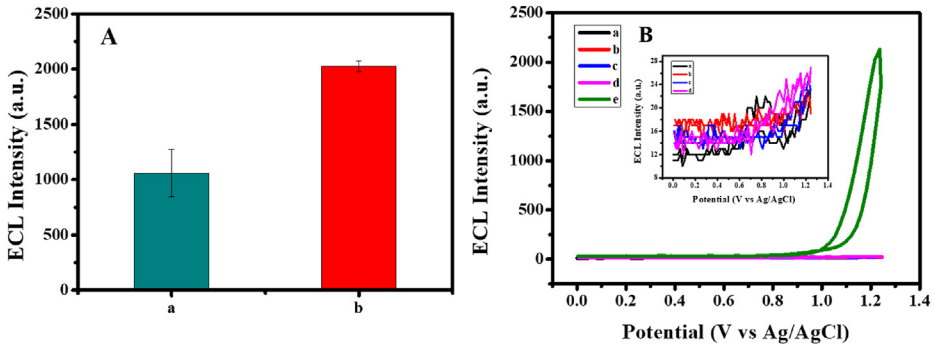

Fig. 3. (A) Comparison of ECL intensity of biosensor without (a) and with (b) the decoration of $Ti_3C_2T_X$ nanosheets with AuNPs. (B) ECL intensity of bare GCE (a), AuNPs/GCE (b), DNA/AuNPs/GCE (c), P-DNA/AuNPs/GCE (d), Ru–$Ti_3C_2T_X$-AuNPs/P-DNA/AuNPs/GCE (e). ECL experiments were performed in a PBS solution (0.1 M, pH 7.4) containing 10 mM TPA. The potential was scanned from 0 to 1.25 V. Scan rate: 0.2 V/s. The concentration of PNK is 1 U mL^{-1}. The inset shows the ECL signals from a to d.

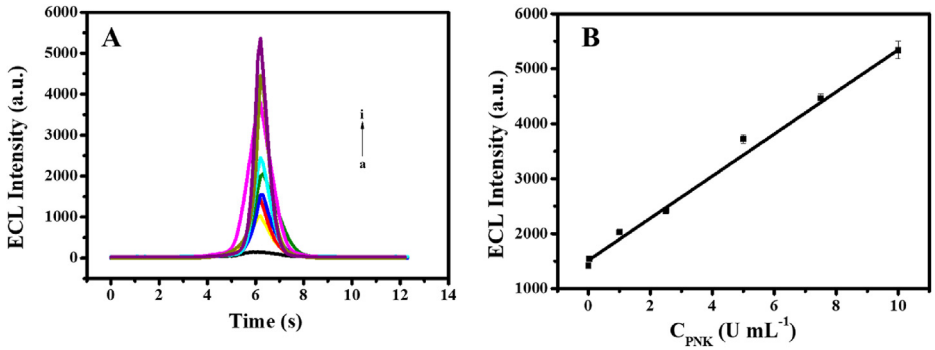

Fig. 4. (A) ECL intensity-time curves of different PNK concentrations. (a–i: 0, 0.0002, 0.002, 0.02, 1.0, 2.5, 5.0, 7.5, 10.0 U mL^{-1}) in a 0.1 M PBS solution (pH 7.4) containing 10 mM TPA. The potential was scanned from 0 to 1.25 V. Scan rate: 0.2 V/s. (B) The linear relationship between ECL intensity and PNK concentrations.

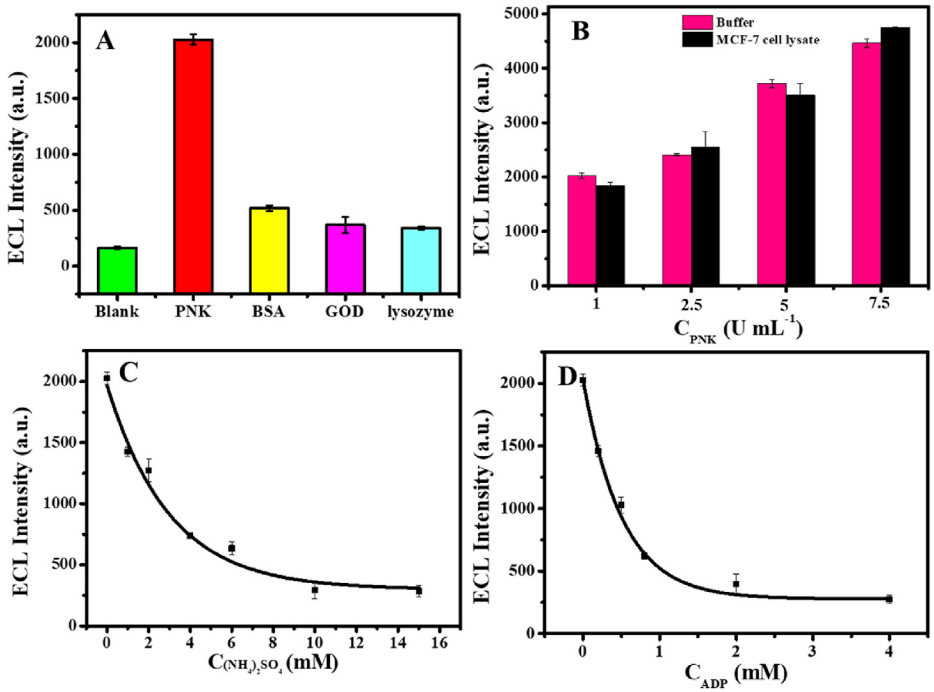

Fig. 5. (A) Selectivity evaluation of the designed biosensor. The 1 U mL^{-1} PNK, 50 μM BSA, 100 μM lysozyme, and 50 μM GOD were tested. (B) Detection of PNK in buffer and MCF-7 cell lysate (n = 3). Inhibition effects of $(NH_4)_2SO_4$ (C) and ADP (D) on the PNK activity, the concentrations of PNK and ATP are 1 U mL^{-1} and 1 mM, respectively. Both tests were performed in solutions containing 10 mM TPA as the coreactant. The potential was scanned from 0 to 1.25 V. Scan rate: 0.2 V/s.

proposed ECL biosensor presents good selectivity for the measurement of PNK activity. In addition, the stable ECL intensity obtained under 10 consecutive scanning cycles with PNK concentration of 1 U mL^{-1} (Fig. S6) and the relative standard deviation (RSD) was 2.40%, confirming that the biosensor presents excellent stability.

3.6. Application in real sample analysis and inhibition assay

In order to evaluate the feasibility of this biosensor for practical sample analysis, the ECL responses in the lysate of Michigan Cancer Foundation-7 cell line (MCF-7) were carried out. They were similar with that in the buffer system (Fig. 5B). Moreover, as demonstrated in Table 1, the recoveries of samples were 98–113%, which demonstrated that the designed ECL sensor was feasible for the sensitive detection of PNK in actual samples. At the same time, the PNK inhibitory activity was evaluated with $(NH_4)_2SO_4$ (Fig. 5C) and ADP (Fig. 5D) as commonly used as antibacterial agents. ADP was selected because it is a non-competitive inhibitor and its inhibition effects are due to its reversible function in the phosphorylation reaction [57]. PNK activity may be suppressed by the $(NH_4)_2SO_4$ reagent, which modify the structure of dsDNA substrate and the spatial conformation of the PNK enzyme [58]. The IC_{50} values for $(NH_4)_2SO_4$ and ADP are 2.549 and 0.442 mM, which are comparable to those previously reported and manifest the practicability of the prepared ECL biosensor for screening PNK inhibitors [59–61].

4. Conclusion

A selective and sensitive ECL biosensor for PNK detection is reported according to the versatility of the structural and electrochemical properties of $Ti_3C_2T_X$ nanomaterial. The $Ti_3C_2T_X$ nanosheets were modified sequentially by AuNPs and then $Ru(bpy)_3^{2+}$ in order to obtain Ru–Ti_3C_2Tx-AuNPs. In situ formation of $Ti_3C_2T_X$-AuNPs provided high catalytic activity rooting in rich Ti vacancy defects. Indeed, the reduction of Au salt thanks to the surface reducibility of Ti leads to the synthesis of AuNPs directly anchored on $Ti_3C_2T_X$. Then, $Ru(bpy)_3^{2+}$ was immobilized on the $Ti_3C_2T_X$-AuNPs by electrostatic interactions between this positively-charged luminophore and the negatively-charge $Ti_3C_2T_X$ nanomaterial to obtain Ru–$Ti_3C_2T_X$-AuNPs. Finally, DNA phosphorylated with PNK was recognized by the chelation between Ti and phosphate groups. PNK was detected with high selectivity without additional identification unit. The designed ECL biosensor with remarkable performances could be applied to detect PNK in MCF-7 cell lysate with recovery rate of 98–113% and a detection limit of 0.0002 U mL^{-1}. This proves that the reported ECL biosensor could be applied to PNK detection in biomedical conditions. The reported biosensor, which combines the remarkable structural and electrochemical properties of $Ti_3C_2T_X$ nanomaterials with the ECL readout should find promising applications in the sensor field dedicated to biomolecular analysis and diagnosis.

Table 1
The activity of PNK in lysate of MCF-7 cells was analyzed by the ECL biosensor.

Sample	Spiked (U mL^{-1})	Found (U mL^{-1})	Recovery (%)	RSD (%)
1	Not Spiked	Not Found	–	–
2	1	0.98	98	3.93
3	2.5	2.69	108	3.45
4	5	5.19	104	6.06
5	7.5	8.45	113	0.17

Funding

This work was financially supported by the Taishan Scholar Program of Shandong Province (ts201511027), the Natural Science Foundation of Shandong Province (ZR2020MB063), China.

Credit authorship contribution statement

Lun Wang: Data curation, Writing – original draft, Investigation, Drafted and revised the manuscript. **Huixin Zhang:** Methodology, Writing – review & editing, Investigation, Design. **Tingting Zhuang:** Characterization, Writing – review & editing. **Jingxu Liu:** Routine analysis. **Neso Sojic:** Characterization, Writing – review & editing. **Zonghua Wang:** Methodology, Writing – review & editing, Supervision, Funding acquisition.

Declaration of competing interest

The authors declare that they have no known competing financial interests or personal relationships that could have appeared to influence the work reported in this paper.

Appendix A. Supplementary data

Supplementary data to this article can be found online at https://doi.org/10.1016/j.aca.2021.339346.

References

[1] J.E. Dick, C. Renault, B.K. Kim, A.J. Bard, Simultaneous detection of single attoliter droplet collisions by electrochemical and electrogenerated chemiluminescent responses, Angew. Chem. Int. Ed. 53 (44) (2014) 11859–11862, https://doi.org/10.1002/anie.201407937.
[2] J. Tan, L.R. Xu, T. Li, B. Su, J.M. Wu, Image-contrast technology based on the electrochemiluminescence of porous silicon and its application in fingerprint visualization, Angew. Chem. Int. Ed. 53 (37) (2014) 9822–9826, https://doi.org/10.1002/anie.201404948.
[3] Z.Y. Liu, W.J. Qi, G.B. Xu, Recent advances in electrochemiluminescence, Chem. Soc. Rev. 44 (10) (2015) 3117–3142, https://doi.org/10.1039/c5cs00086f.
[4] C. Ma, Y. Cao, X.D. Gou, J.J. Zhu, Recent progress in electrochemiluminescence sensing and imaging, Anal. Chem. 92 (1) (2020) 431–454, https://doi.org/10.1021/acs.analchem.9b04947.
[5] N. Sojic, Analytical electrogenerated chemiluminescence: from fundamentals to bioassays, Roy. Soc. Chem. (2020).
[6] E.S. Forzani, D. Lu, M.J. Leright, A.D. Aguilar, F. Tsow, R.A. Iglesias, Q. Zhang, J. Lu, J.H. Li, N.J. Tao, A hybrid electrochemical-colorimetric sensing platform for detection of explosives, J. Am. Chem. Soc. 131 (4) (2009) 1390–1391, https://doi.org/10.1021/ja809104h.
[7] H.J. Wang, R. Yuan, Y.Q. Chai, Y.L. Cao, X.X. Gan, Y.F. Chen, Y. Wang, An ultrasensitive peroxydisulfate electrochemiluminescence immunosensor for streptococcus suis serotype 2 based on L-cysteine combined with mimicking bi-enzyme synergetic catalysis to in situ generate coreactant, Biosens. Bioelectron. 43 (2013) 63–68, https://doi.org/10.1016/j.bios.2012.11.038.
[8] H.R. Zhang, M.S. Wu, J.J. Xu, H.Y. Chen, Signal-On dual-potential electrochemiluminescence based on luminol-gold bifunctional nanoparticles for telomerase detection, Anal. Chem. 86 (8) (2014) 3834–3840, https://doi.org/10.1021/ac403960g.
[9] X.G. Ma, W.Y. Gao, F.X. Du, F. Yuan, J. Yu, Y.R. Guan, N.O. Sojic, G.B. Xu, Rational design of electrochemiluminescent devices, Acc. Chem. Res. 54 (14) (2021) 2936–2945, https://doi.org/10.1021/acs.accounts.1c00230.
[10] M.P. Dinel, S. Tartaggia, G.Q. Wallace, D. Boudreau, J.F. Masson, F. Polo, The fundamentals of real-time surface plasmon resonance/electrogenerated chemiluminescence, Angew. Chem. Int. Ed. 58 (50) (2019) 18202–18206, https://doi.org/10.1002/anie.201909806.
[11] E. Kerr, R. Farr, E.H. Doeven, Y.H. Nai, R. Alexander, R.M. Guijt, B. Prieto-Simon, P.S. Francis, M. Dearnley, D.J. Hayne, L.C. Henderson, N.H. Voelcker, Amplification-free electrochemiluminescence molecular beacon-based microRNA sensing using a mobile phone for detection. https://doi.org/10.1016/j.snb.2020.129261, 2021, 330, 129261.
[12] J.L. Delaney, C.F. Hogan, J.F. Tian, W. Shen, Electrogenerated chemiluminescence detection in paper-based microfluidic sensors. https://doi.org/10.1021/ac102392t, 2011, 83, 4, 1300-1306.
[13] H.L. Qi, C.X. Zhang, Electrogenerated chemiluminescence biosensing, Anal. Chem. 92 (1) (2020) 524–534, https://doi.org/10.1021/acs.analchem.9b03425.
[14] Q.M. Feng, Y.Z. Shen, M.X. Li, Z.L. Zhang, W. Zhao, J.J. Xu, H.Y. Chen, Dual-wavelength electrochemiluminescence ratiometry based on resonance energy

transfer between Au nanoparticles functionalized g-C3N4 nanosheet and Ru(bpy)(3)(2+) for microRNA detection, Anal. Chem. 88 (1) (2016) 937–944, https://doi.org/10.1021/acs.analchem.5b03670.
[15] L. Chen, X.T. Zeng, P. Si, Y.M. Chen, Y.W. Chi, D.H. Kim, G.N. Chen, Gold nanoparticle-graphite-like C3N4 nanosheet nanohybrids used for electrochemiluminescent immunosensor, Anal. Chem. 86 (9) (2014) 4188–4195, https://doi.org/10.1021/10.1021/ac403635f.
[16] A. Zanut, M. Rossetti, M. Marcaccio, F. Ricci, F. Paolucci, A. Porchetta, G. Valenti, DNA-based nanoswitches: insights into electrochemiluminescence signal enhancement, Anal. Chem. 93 (30) (2021) 10397–10402, https://doi.org/10.1021/acs.analchem.1c01683.
[17] L. Zhang, Y. Cheng, J.P. Lei, Y.T. Liu, Q. Hao, H.X. Ju, Stepwise chemical reaction strategy for highly sensitive electrochemiluminescent detection of dopamine, Anal. Chem. 85 (16) (2013) 8001–8007, https://doi.org/10.1021/ac401894w.
[18] Y. Cheng, Y. Huang, J.P. Lei, L. Zhang, H.X. Ju, Design and biosensing of Mg2+-dependent DNAzyme-triggered ratiometric electrochemiluminescence, Anal. Chem. 86 (10) (2014) 5158–5163, https://doi.org/10.1021/ac500965p.
[19] A. Zanut, A. Fiorani, S. Canola, T. Saito, N. Ziebart, S. Rapino, S. Rebeccani, A. Barbon, T. Irie, H.P. Josel, F. Negri, M. Marcaccio, M. Windfuhr, K. Imai, G. Valenti, F. Paolucci, Insights into the mechanism of coreactant electrochemiluminescence facilitating enhanced bioanalytical performance, Nat. Commun. 11 (1) (2020) 2668, https://doi.org/10.1038/s41467-020-16476-2.
[20] S.F. Douman, E. Brennan, E.I. Iwuoha, R.J. Forster, Wireless electrochemiluminescence at Nafion–carbon microparticle composite films, Anal. Chem. 89 (21) (2017) 11614–11619, https://doi.org/10.1021/acs.analchem.7b03040.
[21] W. Guo, H. Ding, C. Gu, Y. Liu, X. Jiang, B. Su, Y. Shao, Potential-resolved multicolor electrochemiluminescence for multiplex immunoassay in a single sample, J. Am. Ceram. Soc. 140 (46) (2018) 15904–15915, https://doi.org/10.1021/jacs.8b09422.
[22] Y. Zhao, J. Yu, G. Xu, N. Sojic, G. Loget, Photoinduced electrochemiluminescence at silicon electrodes in water, J. Am. Chem. Soc. 141 (2019) 13013, https://doi.org/10.1021/jacs.9b06743.
[23] X. Liu, L. Shi, W. Niu, H. Li, G. Xu, Environmentally friendly and highly sensitive Ruthenium(II) Tris(2,2'-bipyridyl) electrochemiluminescent system using 2-(Dibutylamino) ethanol as co-reactant, Angew. Chem. Int. Ed. 46 (3) (2007) 421–424, https://doi.org/10.1002/anie.200603491.
[24] S. Carrara, A. Aliprandi, C.F. Hogan, L. De Cola, Aggregation-induced electrochemiluminescence of platinum(II) complexes, J. Am. Chem. Soc. 139 (41) (2017) 14605–14610, https://doi.org/10.1021/jacs.7b07710.
[25] S. Carrara, F. Arcudi, M. Prato, L. De Cola, Amine-rich nitrogen-doped carbon nanodots as platform for self-enhancing electrochemiluminescence, Angew. Chem. Int. Ed. 56 (17) (2017) 4757–4761, https://doi.org/10.1002/anie.201611879.
[26] J.M. Fernandez-Hernandez, E. Longhi, R. Cysewski, F. Polo, H.P. Josel, L. De Cola, Photophysics and electrochemiluminescence of bright cyclometalated Ir(III) complexes in aqueous solutions, Anal. Chem. 88 (8) (2016) 4174–4178, https://doi.org/10.1021/acs.analchem.6b00312.
[27] F. Polo, F. Rizzo, M. Veiga-Gutierrez, L. De Cola, S. Quici, Efficient greenish blue electrochemiluminescence from fluorene and spirobifluorene derivatives, J. Am. Ceram. Soc. 134 (37) (2012) 15402–15409, https://doi.org/10.1021/ja3054018.
[28] L. Chen, D.J. Hayne, E.H. Doeven, J. Agugiaro, D.J.D. Wilson, L.C. Henderson, T.U. Connell, Y.H. Nai, R. Alexander, S. Carrara, C.F. Hogan, P.S. Donnelly, P.S. Francis, A conceptual framework for the development of iridium(III) complex-based electrogenerated chemiluminescence labels, Chem. Sci. 10 (37) (2019) 8654–8667, https://doi.org/10.1039/c9sc01391a.
[29] N. Wang, H. Gao, Y. Li, G. Li, W. Chen, Z. Jin, J. Lei, Q. Wei, H. Ju, Dual intramolecular electron transfer for in situ coreactant-embedded electrochemiluminescence microimaging of membrane protein, Angew. Chem. Int. Ed. 60 (1) (2021) 197–201, https://doi.org/10.1002/anie.202011176.
[30] H. Li, A.C. Sedgwick, M. Li, R.A.R. Blackburn, S.D. Bull, S. Arbault, T.D. James, N. Sojic, Selective electrochemiluminescent sensing of saccharides using boronic acid-modified coreactant, Chem. Commun. 52 (87) (2016) 12845–12848, https://doi.org/10.1039/c6cc07030b.
[31] A. Fiorani Irkham, G. Valenti, N. Kamoshida, F. Paolucci, Y. Einaga, Electrogenerated chemiluminescence by in situ production of coreactant hydrogen peroxide in carbonate aqueous solution at a boron-doped diamond electrode, J. Am. Chem. Soc. 142 (3) (2020) 1518–1525, https://doi.org/10.1021/jacs.9611842.
[32] X. Zhong, S.S. Yang, N. Liao, R. Yuan, Y. Zhuo, Development of hollow electrochemiluminescent nanocubes combined with a multisite-anchored DNA nanomachine for mycotoxin detection, Anal. Chem. 93 (12) (2021) 5301–5308, https://doi.org/10.1021/acs.analchem.1c00446.
[33] P.F. Liu, K.R. Zhao, Z.J. Liu, L. Wang, S.Y. Ye, G.X. Liang, Cas12a-based electrochemiluminescence biosensor for target amplification-free DNA detection, Biosens. Bioelectron. 176 (2021) 112954, https://doi.org/10.1016/j.bios.2020.112954.
[34] P. Sun, M. Wang, L. Liu, L.P. Jiao, W. Du, F. Xia, M.J. Liu, Sensitivity enhancement of surface plasmon resonance biosensor based on graphene and barium titanate layers, Appl. Surf. Sci. 475 (2019) 342–347.
[35] Z.H. Wang, Z.Y. Yan, N. Sun, Y. Liu, Multiple signal amplification electrogenerated chemiluminescence biosensors for sensitive protein kinase activity analysis and inhibition, Biosens. Bioelectron. 68 (2015) 771–776, https://doi.org/10.1016/j.bios.2015.02.006.
[36] P. Bertoncello, R.J. Forster, Nanostructured materials for electrochemiluminescence (ECL)-based detection methods: recent advances and future perspectives, Biosens. Bioelectron. 24 (11) (2009) 3191–3200, https://doi.org/10.1016/j.bios.2009.02.013.
[37] P. Bertoncello, A. Stewart, L. Dennany, Analytical applications of nanomaterials in electrogenerated chemiluminescence, Anal. Bioanal. Chem. 406 (23) (2014) 5573–5587, https://doi.org/10.1007/s00216-014-7946-x.
[38] S. Deng, H. Ju, Electrogenerated chemiluminescence of nanomaterials for bioanalysis, Analyst 138 (1) (2013) 43–61, https://doi.org/10.1039/c2an36122a.
[39] P. Bertoncello, P. Ugo, Recent advances in electrochemiluminescence with quantum dots and arrays of nanoelectrodes, ChemElectroChem 4 (7) (2017) 1663–1676, https://doi.org/10.1002/celc.201700201.
[40] J.W. Sun, H. Sun, Z.Q. Liang, Nanomaterials in electrochemiluminescence sensors, ChemElectroChem 4 (7) (2017) 1651–1662, https://doi.org/10.1002/celc.201600920.
[41] M. Naguib, J. Come, B. Dyatkin, V. Presser, P.L. Taberna, P. Simon, M.W. Barsoum, Y. Gogotsi, MXene: a promising transition metal carbide anode for lithium-ion batteries, Electrochem. Commun. 16 (1) (2012) 61–64, https://doi.org/10.1016/j.elecom.2012.01.002.
[42] H.W. Wang, M. Naguib, K. Page, D.J. Wesolowski, Y. Gogotsi, Resolving the structure of Ti3C2Tx MXenes through multilevel structural modeling of the atomic pair distribution function, Chem. Mater. 28 (1) (2016) 349–359, https://doi.org/10.1021/acs.chemmater.5b04250.
[43] H.X. Zhang, Z.H. Wang, Q.X. Zhang, F. Wang, Y. Liu, Ti3C2 MXenes nanosheets catalyzed highly efficient electrogenerated chemiluminescence biosensor for the detection of exosomes, Biosens. Bioelectron. 124 (2019) 184–190, https://doi.org/10.1016/j.bios.2018.10.016.
[44] Y.F. Fang, X.C. Yang, T. Chen, G.F. Xu, M.L. Liu, J.Q. Liu, Y.H. Xu, Two-dimensional titanium carbide (MXene)-based solid-state electrochemiluminescent sensor for label-free single-nucleotide mismatch discrimination in human Urine, Sensor. Actuator. B Chem. 263 (2018) 400–407, https://doi.org/10.1016/j.snb.2018.02.102.
[45] J.Z. Zhang, E. Kerr, K.A.S. Usman, E.H. Doeven, P.S. Francis, L.C. Henderson, J.M. Razal, Cathodic electrogenerated chemiluminescence of tris(2,2 '-bipyridine)ruthenium(ii) and peroxydisulfate at pure Ti(3)C(2)T(x)MXene electrodes, Chem. Commun. 56 (69) (2020) 10022–10025, https://doi.org/10.1039/d0cc02993a.
[46] Y. Sun, Y.M. Zhang, H.X. Zhang, M.L. Liu, Y. Liu, Integrating highly efficient recognition and signal transition of g-C3N4 embellished Ti3C2 MXene hybrid nanosheets for electrogenerated chemiluminescence analysis of protein kinase activity, Anal. Chem. 92 (15) (2020) 10668–10676, https://doi.org/10.1021/acs.analchem.0c01776.
[47] H.X. Zhang, Z.H. Wang, F. Wang, Y.M. Zhang, H.Y. Wang, Y. Liu, In situ formation of gold nanoparticles decorated Ti3C2 MXenes nanoprobe for highly sensitive electrogenerated chemiluminescence detection of exosomes and their surface proteins, Anal. Chem. 92 (7) (2020) 5546–5553, https://doi.org/10.1021/acs.analchem.0c00469.
[48] V.M.H. Ng, H. Huang, K. Zhou, P.S. Lee, W.X. Que, J.Z. Xu, L.B. Kong, Recent progress in layered transition metal carbides and/or nitrides (MXenes) and their composites: synthesis and applications, J. Mater. Chem. A. 5 (18) (2017) 8769, https://doi.org/10.1039/c7ta90088k.
[49] M. Naguib, M. Kurtoglu, V. Presser, J. Lu, J.J. Niu, M. Heon, L. Hultman, Y. Gogotsi, M.W. Barsoum, Two-dimensional nanocrystals produced by exfoliation of Ti3AlC2, Adv. Mater. 23 (37) (2011) 4248–4253, https://doi.org/10.1002/adma.201102306.
[50] M. Naguib, V.N. Mochalin, M.W. Barsoum, Y. Gogotsi, 25th anniversary article: MXenes: a new family of two-dimensional materials, Adv. Mater. 26 (7) (2014) 992–1005, https://doi.org/10.1002/adma.201304138.
[51] X.H. Zhu, Y.Y. Zhang, M.L. Liu, Y. Liu, 2D titanium carbide MXenes as emerging optical biosensing platforms, Biosens. Bioelectron. 171 (2021) 112730, https://doi.org/10.1016/j.bios.2020.112730.
[52] J. Halim, S. Kota, M.R. Lukatskaya, M. Naguib, M.Q. Zhao, E.J. Moon, Synthesis and characterization of 2D molybdenum carbide (MXene), Adv. Funct. Mater. 26 (18) (2016) 3118–3127, https://doi.org/10.1002/adfm.201505328.
[53] Y. Xie, M. Naguib, V.N. Mochalin, M.W. Barsoum, Y. Gogotsi, X.Q. Yu, Role of surface structure on Li-ion energy storage capacity of two-dimensional transition-metal carbides, J. Am. Chem. Soc. 136 (17) (2014) 6385–6394, https://doi.org/10.1021/ja501520b.
[54] A. Sinha, Dhanjai, H.M. Zhao, Y.J. Huang, X.B. Lu, J.P. Chen, R. Jain, MXene: an emerging material for sensing and biosensing, Trends Anal. Chem. 105 (2018) 424–435, https://doi.org/10.1016/j.trac.2018.05.021.
[55] J. Ma, Jiang, Q. Jiang, Y.N. Zhou, W. Chu, S. Perathoner, C.F. Jiang, K.H. Wu, G. Centi, Y.F. Liu, Tuning the chemical properties of Co-Ti3C2Tx MXene materials for catalytic CO2 reduction, Small 17 (26) (2021) 2007509, https://doi.org/10.1002/smll.202007509.
[56] G.Y. Zhang, H.N. Chai, M.W. Tian, S.F. Zhu, L.J. Qu, X.J. Zhang, Zirconium–Metalloporphyrin Frameworks–Luminol competitive electrochemiluminescence for ratiometric detection of polynucleotide kinase activity, Anal. Chem. 92 (2020) 7354–7362, https://doi.org/10.1021/acs.analchem.0c01262.
[57] C.B. Ma, E.S. Yeung, Highly sensitive detection of DNA phosphorylation by counting single nanoparticles, Anal. Bioanal. Chem. 397 (6) (2010) 2279–2284, https://doi.org/10.1007/s00216-010-3801-x.
[58] V. Cameron, O.C. Uhlenbeck, 3 ' -phosphatase activity in T4 polynucleotide

kinase, Biochemistry 16 (1977) 5120–5126, https://doi.org/10.1021/bi00642a027.
[59] J. Xu, Y.F. Gao, B.X. Li, Y. Jin, Cyclic up-regulation fluorescence of pyrene excimer for studying polynucleotide kinase activity based on dual amplification, Biosens. Bioelectron. 80 (2016) 91–97, https://doi.org/10.1016/j.bios.2016.01.046.
[60] L. Cui, J. Hu, M. Wang, X.K. Diao, C.C. Li, C.Y. Zhang, Mimic peroxidase- and Bi2S3 nanorod-based photoelectrochemical biosensor for signal-on detection of polynucleotide kinase, Anal. Chem. 90 (19) (2018) 11478–11485, https://doi.org/10.1021/acs.analchem.8b02673.
[61] L.J. Wang, Q.Y. Zhang, B. Tang, C.Y. Zhang, Single-molecule detection of polynucleotide kinase based on phosphorylation-directed recovery of fluorescence quenched by Au nanoparticles, Anal. Chem. 89 (13) (2017) 7255–7261, https://doi.org/10.1021/acs.analchem.7b01783.